ACS OMEGA

Open Access



http://pubs.acs.org/journal/acsodf

Article

# Proteomic Insights into IgA Nephropathy: A Comprehensive Analysis of Differentially Expressed Proteins in the Kidney

Jingxian Huang,[#] Hongguo Zhu,[#] Shanshan Li,[#] Jing Qiu, Hougang Yang, Fengping Zheng, Zhifeng Luo, Qiang Yan, Fanna Liu, Lianghong Yin,[*] Donge Tang,[*] and Yong Dai[*]

Cite This: *ACS Omega* 2025, 10, 17208−17220

Read Online

ACCESS | Metrics & More | Article Recommendations | Supporting Information

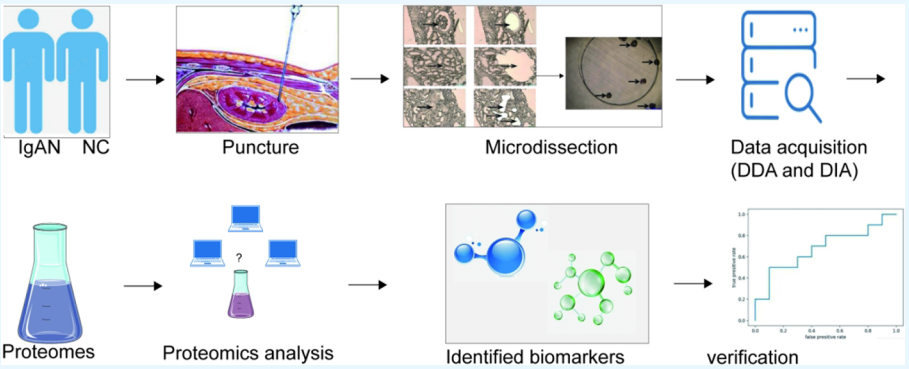


**ABSTRACT:** IgA nephropathy represents a significant challenge in nephrology research, and an understanding of its underlying molecular mechanisms is crucial. In this study, we conducted a comprehensive proteomic investigation of IgA nephropathy utilizing microdissection techniques combined with data-independent acquisition technology. Our analysis focused on differentially expressed proteins in the glomeruli, interstitium, and tubules of the kidney. Functional enrichment analysis revealed distinct pathway enrichment patterns, with fatty acid synthesis predominating in the glomerulus and complement and coagulation pathways predominantly enriched in the tubules. These pathway enrichments suggest potential key contributors to the pathogenesis of IgA nephropathy. Furthermore, our study identified ATP1B1 and COX4I1 in the glomerulus and SLC22A13 in the tubules as promising diagnostic markers for the disease. Meanwhile, C4A and APEX1 proteins were identified as valuable biomarkers for assessing disease progression. This research could provide valuable insights into the proteomic alterations associated with IgA nephropathy and offer potential targets for further therapeutic exploration.

## 1. INTRODUCTION

IgA nephropathy (IgAN), universally acknowledged as the predominant form of primary glomerulonephritis, significantly contributes to the incidence and progression of chronic kidney disease (CKD) and end-stage renal disease (ESRD).[1−6] Research shows that approximately 30−40% of patients with IgAN are likely to develop ESRD within 20−30 years following their initial diagnosis.[2] Globally, the annual incidence rate of IgAN in adults is estimated at about 2.5 cases per 100,000 individuals.[7] Notably, there is a distinct geographic variance in the distribution of this disease, with East Asia reporting the highest incidence rates.[8] In China, for instance, IgAN constitutes about 45% of all primary glomerular cases.[9] IgAN predominantly affects young adults, with a higher incidence in males.[3,10,11] The clinical presentation of IgAN varies widely, encompassing a spectrum from asymptomatic microscopic hematuria to substantial proteinuria, and can include a rapid decline in renal function.[5] At present, the diagnosis of IgAN is dependent on histopathological analysis of renal biopsy samples, and as of yet, there are no treatments specifically targeting IgAN.[2,12,13] The prognosis for IgAN patients varies widely.[14,15] Despite considerable advancements in understanding its pathogenesis, current knowledge still falls short of fully explaining the pathogenic mechanism of the disease.[4,16−18] Renal biopsy continues to be the definitive diagnostic standard for glomerular diseases such as IgAN.

Laser capture microdissection (LCM) is a pivotal method enabling researchers to isolate specific tissues or cells under direct microscopic observation. The high purity of LCM-derived samples makes them ideal for a range of downstream assays, such as proteomic and genomic analyses.[19,20] Applicable to various

Received: September 18, 2024
Revised: April 10, 2025
Accepted: April 14, 2025
Published: April 24, 2025

specimen types, LCM has significantly enhanced research capabilities.[19] In parallel, mass spectrometry-based proteomics has evolved into a vital tool in both biological and medical research.[21,22] In recent years, data-independent acquisition (DIA)-based sequential window acquisition of all theoretical mass spectra (SWATH-MS), the next-generation proteomic method, is an emerging strategy, which combines the deep proteome coverage capability with a favorable quantitative accuracy and reproducibility.[23−30] SWATH-MS has also been applied to the scientific research projects such as plasma proteomics,[31] microbe proteomics,[29,32] and tissue proteomics.[33] For kidney diseases, it is turned out to be feasible and of great clinical value to use LCM coupled with mass spectrometry-based proteomics to investigate the potential biomarkers,[34−37] classification of disease,[38] glomerular components,[39−41] and pathogenic mechanisms.[42] To date, the mechanisms of occurrence and development of IgAN have not been fully understood. In addition, kidney biopsy tissue is the sample source of interest in the study of the disease. Therefore, in the present investigation, we employed LCM combined with SWATH-MS to identify the changed protein expression profiles of the glomerulus, tubule, and interstitium in IgAN patients, and then bioinformatic analyses were performed on these changed proteins, which may play a positive role in our better understanding of the disease.

## 2. RESULTS

**2.1. Patient Characteristics.** The clinical characteristics of patients with IgAN ($n$ = 18) and normal control kidney tissues collected from the para-cancer tissue of the renal carcinoma without pathological changes and invasion (NC) ($n$ = 11) are shown in Table 1. The detailed clinical information is provided in Table S1.

**Table 1. Clinical Characteristics of Patients**[a]

| | IgAN | NC |
|---|---|---|
| age (years) | 36.17 ± 9.52 | 38.5 ± 5.4 |
| sex (female/male) | 10/7 | 0/11 |
| systolic blood pressure (mm Hg) | 125.94 ± 20.40 | 102.27 ± 4.47 |
| diastolic blood pressure (mm Hg) | 80.06 ± 14.49 | 72.36 ± 8.17 |
| blood urea (mmol/L) | 6.88 ± 5.72 | NA |
| serum creatinine (μmol/L) | 94.44 ± 56.89 | 97.14 ± 21.43 |
| blood uric acid (μmol/L) | 407.23 ± 158.60 | 360.56 ± 34.99 |
| serum albumin (g/L) | 37.39 ± 5.48 | 30.46 ± 5.45 |
| total cholesterol (mmol/L) | 5.13 ± 1.56 | 5.15 ± 0.58 |
| triglyceride (mmol/L) | 1.46 ± 0.49 | 1.60 ± 0.33 |
| 24-h urinary protein quantity (g) | 1.21 ± 1.13 | NA |

[a]Data are presented as the mean ± SD. NA − not available.

**2.2. Proteomics Profiling from IgAN Patients versus NC in the Glomerulus, Tubules, and Interstitium.** The initial mass spectrometry data collection was performed in the data-dependent acquisition (DDA) mode. Our spectral library encompassed 81,369 peptides and 8310 proteins. The DDA results, including distributions of unique peptides, protein mass, and coverage, are presented in Figure S1A. A total of 86 samples provided (MS) data in DIA mode, leading to the quantitation of 50,894 peptides and 2982 proteins. Quantitative data of each sample is summarized in Figure S1B. In this research, MSstats software was utilized for correcting intrasystem errors and normalizing each sample, and the Limma package in R was used to identify differentially expressed proteins (DEPs). The significance of DEPs was assessed based on predetermined comparison groups and a linear mixed-effect model. We applied two filtering criteria: a fold change greater than 1.5 and a $p$-value less than 0.05 to identify significant DEPs. Following these criteria, we identified 112 proteins as significantly upregulated and 74 as significantly downregulated in the glomerulus of IgAN patients compared to the control group (IgAN-G/CG-G), as seen in Figure 1A. In the tubular region (IgAN-T/CG-T), there were 266 proteins significantly upregulated and 126 downregulated, as depicted in Figure 1B. The interstitial area (IgAN-I/CG-I) showed 231 DEPs, with 113 being upregulated and 118 downregulated, as illustrated in Figure 1C. DEPs of three regions of the glomerulus, renal tubules, and renal interstitium are presented in Tables S2−S4. Through the intersection of the three groups of DEPs, surprisingly, only three proteins were found to be shared in the three regions: FABP1, DYSF, and HSPA1A. We also found 135 proteins that were unique to the glomerulus, 311 proteins that were unique to the renal tubules, and 164 proteins that were unique to the renal interstitium. This thorough analysis sheds light on the specific protein expression changes in IgAN and aids in understanding the molecular underpinnings of the disease.

**2.3. Function Analysis Patterns Characterized by Different Regions of the Kidney.** To elucidate the roles of DEPs (including both upregulated and downregulated proteins) in IgAN versus NC, we conducted Gene Ontology (GO) and Kyoto Encyclopedia of Genes and Genomes (KEGG) enrichment analyses. These analyses focused on DEPs across three distinct renal regions: the glomerulus, renal tubules, and renal interstitium. GO enrichment results revealed specific pathway enrichments in each region. The glomerulus predominantly exhibited enrichment in the energy and metabolic pathways (Figure 2A), whereas the renal tubules showed a significant enrichment in the immunity and inflammation pathways (Figure 2B). The renal interstitium was primarily enriched in the adherence and extracellular matrix (ECM) interaction pathways (Figure 2C). In parallel, KEGG enrichment analysis provided insights into unique pathway involvements. By the KEGG enrichment analysis, we found that three regions of the kidney mainly showed metabolic disorders (Tables S5−S7). Additionally, we found that both the glomerulus and the renal tubules were involved in fatty acid metabolism disorders, but this was not found in the renal interstitium. We also found that immune-related pathways were enriched in the renal tubules and interstitium but not significantly enriched in the glomerulus. We took a heatmap of these pathways; the glomerulus uniquely showed involvement in the fatty acid biosynthesis and fat digestion and absorption pathways. Meanwhile, the tubules uniquely exhibited involvement in the phagosome and complement and coagulation cascade pathways (Figure 2D). These results suggest that abnormal fatty acid biosynthesis was more prominent in the glomerulus than in other regions, while complement and coagulation cascades were more prominent in the renal tubules. We did not find a specific signaling pathway for its expression in the renal interstitium, but we found that the ECM−receptor interaction pathway is particularly enriched. Studies had shown that ECM accumulation was a key feature of renal interstitial fibrosis, and the inhibition of ECM−receptor interactions could reduce collagen deposition and thus inhibit interstitial fibrosis.[43,44] Therefore, we believe that the ECM−receptor interaction may be an important influencing factor of IgAN renal interstitial fibrosis. Further, we conducted a gene set enrichment analysis (GSEA) on these pathways of


https://doi.org/10.1021/acsomega.4c07827
ACS Omega 2025, 10, 17208−17220

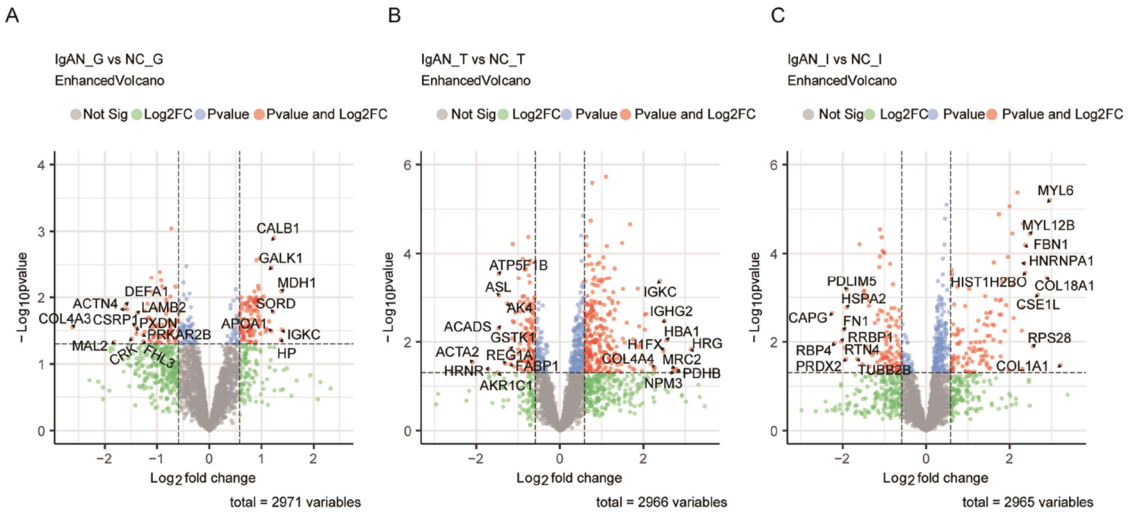


**Figure 1.** Analysis of DEPs in different regions of the kidney. Volcano plots from different kidney compartments: (A) glomerulus, (B) tubules, and (C) interstitium.

interest. This analysis revealed that the fatty acid elongation pathway was activated in the glomerulus (Figure 2E), the complement and coagulation cascade pathways were notably activated in the tubules (Figure 2F), and the ECM−receptor interaction pathway showed significant activation in the renal interstitium (Figure 2G). In addition, in a proteomics study of IgAN urine, the complement and coagulation cascade and ECM−receptor interaction pathway played an important role in the pathogenesis of IgAN.[45] This also suggests that these two pathways may be related to the pathogenesis of IgAN. These findings provide a deeper understanding of the molecular mechanisms and pathway involvement in different regions of the kidney in IgAN.

**2.4. Identification of Co-Expression Protein Modules and Screening of Diagnostic Biomarkers in the Glomerulus.** In the glomerular dataset, we used WGCNA to identify protein modules co-expressed by numerous proteins. First, we considered the sample type as a clinical trait: the IgAN group ($n$ = 18) and the normal group ($n$ = 11). Then, based on a scale independence of >0.9, we selected 10 as the soft threshold power $\beta$ to ensure a biologically significant scale-free network (Figure 3A). Through hierarchical clustering analysis and the dynamic tree cut method of gene dendrograms, proteins were grouped into nine modules, as shown in Figure 3B, with the blue, brown, and turquoise modules showing significant association with IgAN, which were selected for further analysis. A total of 340 proteins were significantly associated with the IgAN protein significance and module membership. By utilizing a Venn diagram to compare the overlapping regions of DEGs and key module proteins, we identified 81 overlapping protein regions (Figure 3C). We used two machine-learning algorithms to identify feature genes: SVM-RFE selected 19 predicted proteins (Figure 3D) and LASSO regression analysis selected 8 predicted proteins from among the statistically significant univariate variables (Figure 3E). Both algorithms identified ATP1B1, CALB1, and COX4I1 as overlapping proteins (Figure 3F). In the glomerulus, the expression of ATP1B1, CALB1, and COX4I1 was considerably higher in the IgAN group than in the control group (Figure 3G). The receiver operating characteristic (ROC) curves for ATP1B1, CALB1, and COX4I1, with AUCs of 0.778, 0.838, and 0.780, respectively, indicated that these biological markers have high predictive accuracy (Figure 3H).

**2.5. Identification of Co-Expression Protein Modules and Screening of Diagnostic Biomarkers in the Tubules.** Similarly, in the renal tubule dataset, we used WGCNA to identify protein modules co-expressed by numerous proteins. First, we considered the sample type as a clinical trait: the IgAN group ($n$ = 18) and the normal group ($n$ = 11). Based on a scale independence of >0.9, we selected 6 as the soft threshold power $\beta$ to ensure a biologically significant scale-free network (Figure 4A). Through hierarchical clustering analysis and the dynamic tree cut method of gene dendrograms, proteins were grouped into eight modules, as shown in Figure 4B, with the purple module showing significant associations with IgAN, which were selected for further analysis. A total of 175 proteins were significantly associated with the IgAN protein significance and module membership. Using a Venn diagram to compare the overlapping regions of DEGs and key module proteins, we identified 20 overlapping protein regions (Figure 4C). Two machine-learning algorithms were employed to identify feature genes: SVM-RFE selected 13 predicted proteins (Figure 4D) and LASSO regression analysis identified 7 predicted proteins from among the statistically significant univariate variables (Figure 4E). Both algorithms identified CCAR1, FMO6P, NUDT12, SLC22A13, TECR, and WASF2 as overlapping proteins (Figure 4F). In the tubules, the expression levels of CCAR1, FMO6P, NUDT2, SLC22A13, TECR, and WASF2 were considerably higher in the IgAN group compared to the control group (Figure 4G). The ROC curves for CCAR1, FMO6P, NUDT12, SLC22A13, TECR, and WASF2 with AUCs of 0.831, 0.965, 0.864, 0.894, 0.904, and 0.909, respectively, indicated that these biological markers have high predictive accuracy (Figure 4H).

**2.6. Validation of Diagnostic Markers.** To validate the accuracy of the diagnostic biomarkers, we assessed the diagnostic effectiveness of two proteins in the glomerulus using the validation dataset. The AUC values for the biomarkers ATP1B1 and COX4I1 were found to be 0.761 and 0.821, respectively (Figure 5A). Similarly, in the tubules, we verified the diagnostic effectiveness of one protein in the validation dataset, discovering that the AUC value for the biomarker SLC22A13 was 0.917 (Figure 5B).



https://doi.org/10.1021/acsomega.4c07827
ACS Omega 2025, 10, 17208−17220

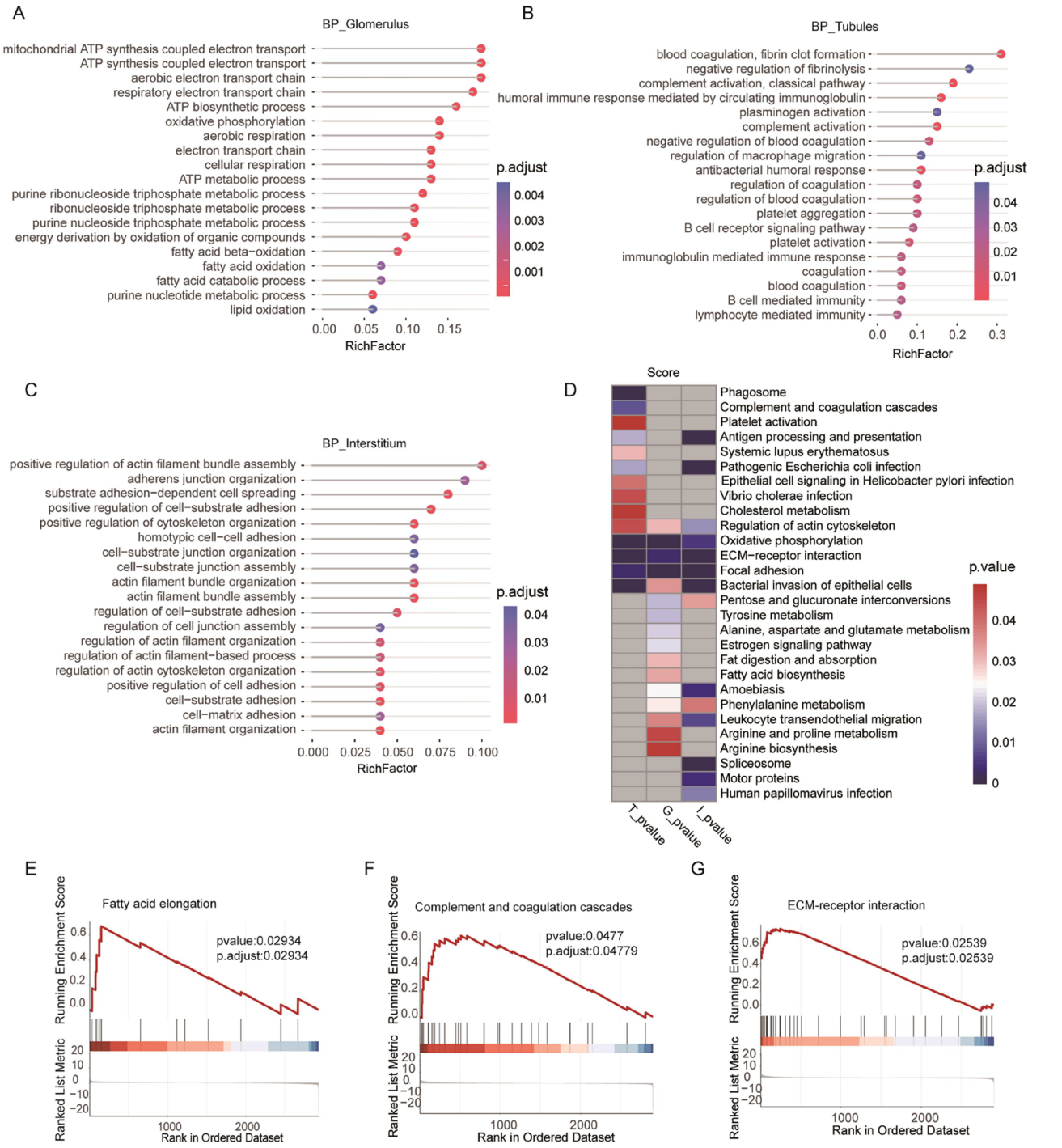


**Figure 2.** Function analysis in different regions of the kidney. The GO enrichment analysis in DEPs of different kidney compartments: (A) glomerulus, (B) tubules, and (C) interstitium. The *x*-axis represents the enrichment factor (RichFactor), which was calculated by dividing the number of DEPs annotated to each pathway by the total number of identified proteins annotated to that specific pathway. A higher RichFactor indicated a greater proportion of DEPs associated with the pathway. (D) Comparison of KEGG pathways of DEPs from the renal glomerulus, tubules, and interstitium. The light gray color indicates not available (N/A). (E) GSEA enrichment plots of the fatty acid degradation pathway in the glomerulus. (F) GSEA enrichment plots of complement and coagulation cascade pathways in tubules. (G) GSEA enrichment plots of the ECM−receptor interaction pathway in the interstitium.

**2.7. Molecular Functions of Key Proteins in the Glomerular and Tubular Tissues as Revealed by GSVA Correlation Analysis.** To further elucidate the molecular functions of key proteins, we conducted a gene set variation analysis (GSVA) to assess correlations with key proteins in the glomerular and tubular tissues. The results showed that in the glomerulus, ATP1B1 and COX4I1 were significantly positively correlated with fatty acid metabolism, adipogenesis, and oxidative phosphorylation. Notably, ATP1B1 was also positively correlated with the glycolysis pathway (Figure 6A), suggesting that ATP1B1 and COX4I1 played important roles in the metabolic processes of the glomerulus. In the tubules,



https://doi.org/10.1021/acsomega.4c07827
ACS Omega 2025, 10, 17208−17220

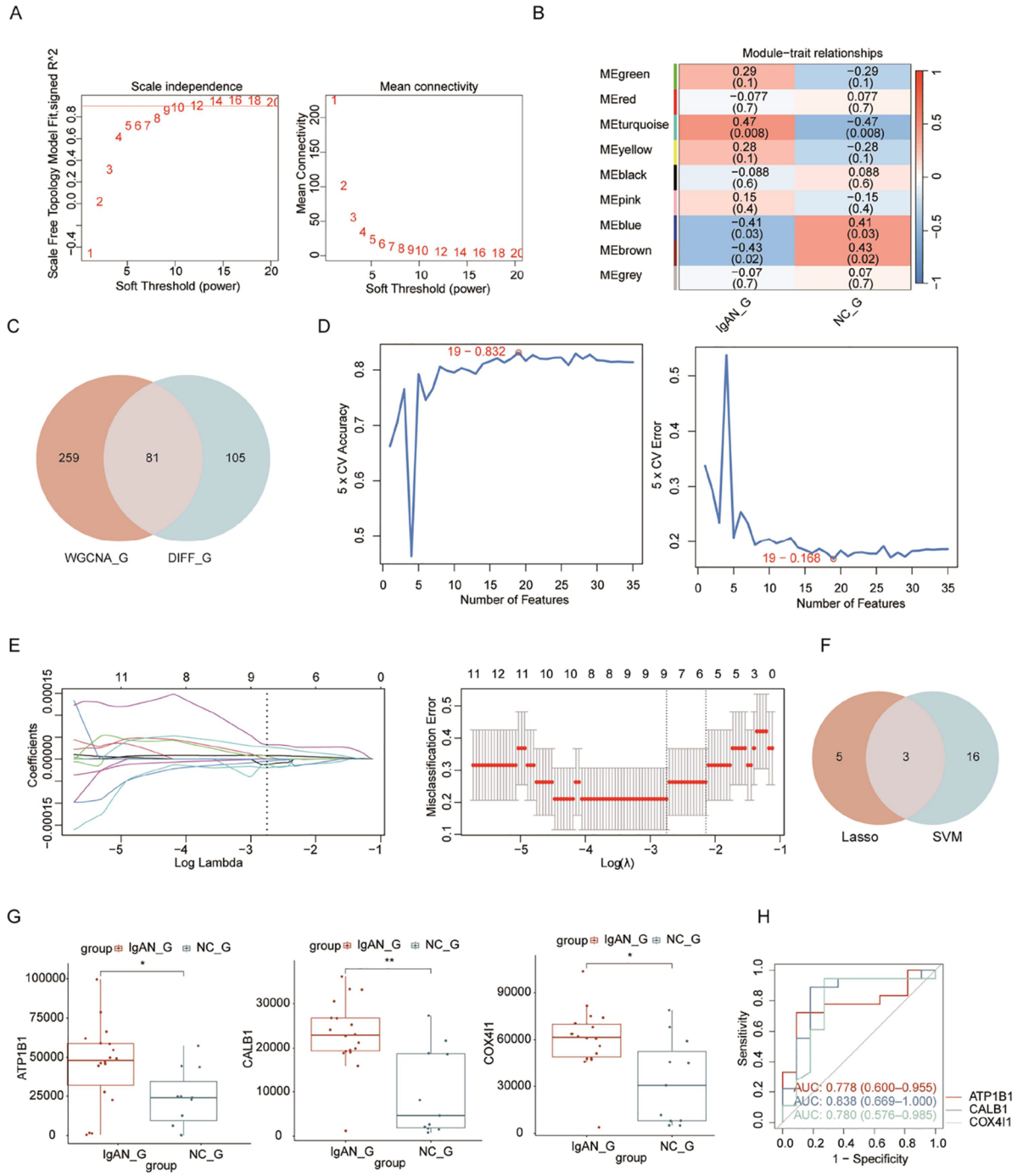


**Figure 3.** Screening of diagnostic markers by WGCNA and machine learning in the glomerulus. (A) Analysis of the network topology for various soft threshold values. (B) Relationship between modules and clinical traits. The colors represent the correlation coefficient. (C) Venn diagram of key module proteins and DEPs. (D) Screening of biomarkers using the SVM-RFE algorithm. (E) LASSO logistic regression algorithm to identify diagnostic markers. (F) Venn diagram showing the overlap of diagnostic markers identified by both algorithms. (G) Boxplot illustrating the expression levels of hub genes between the IgAN group and the control group. *$p < 0.05$, **$p < 0.01$, ***$p < 0.001$. (H) ROC curve with AUC and 95%CI demonstrating the diagnostic efficacy of the identified biomarkers.

SLC22A13 was negatively correlated to PI3K/AKT signaling and TNF-$\alpha$/NF-$\kappa$B signaling pathways. This suggested that SLC22A13 probably played an important role in the proliferation and differentiation of renal tubular cells. At the same time, we also found a positive correlation between SLC22A13 and the complement and inflammation response pathways, but it was not statistically significant.

**2.8. Alterations in Proteomics Linked to the Exacerbation of Disease in Patients with IgAN.** To elucidate the variations in protein expression associated with the exacerbation of IgAN, we employed the short-time-series expression miner (STEM) analysis. This approach was applied to NC, as well as IgAN stages II, III, and IV, to derive distinct profiles characterizing the behavior of protein expression. We discerned four distinct protein profiles exhibiting varied expression


https://doi.org/10.1021/acsomega.4c07827
ACS Omega 2025, 10, 17208−17220

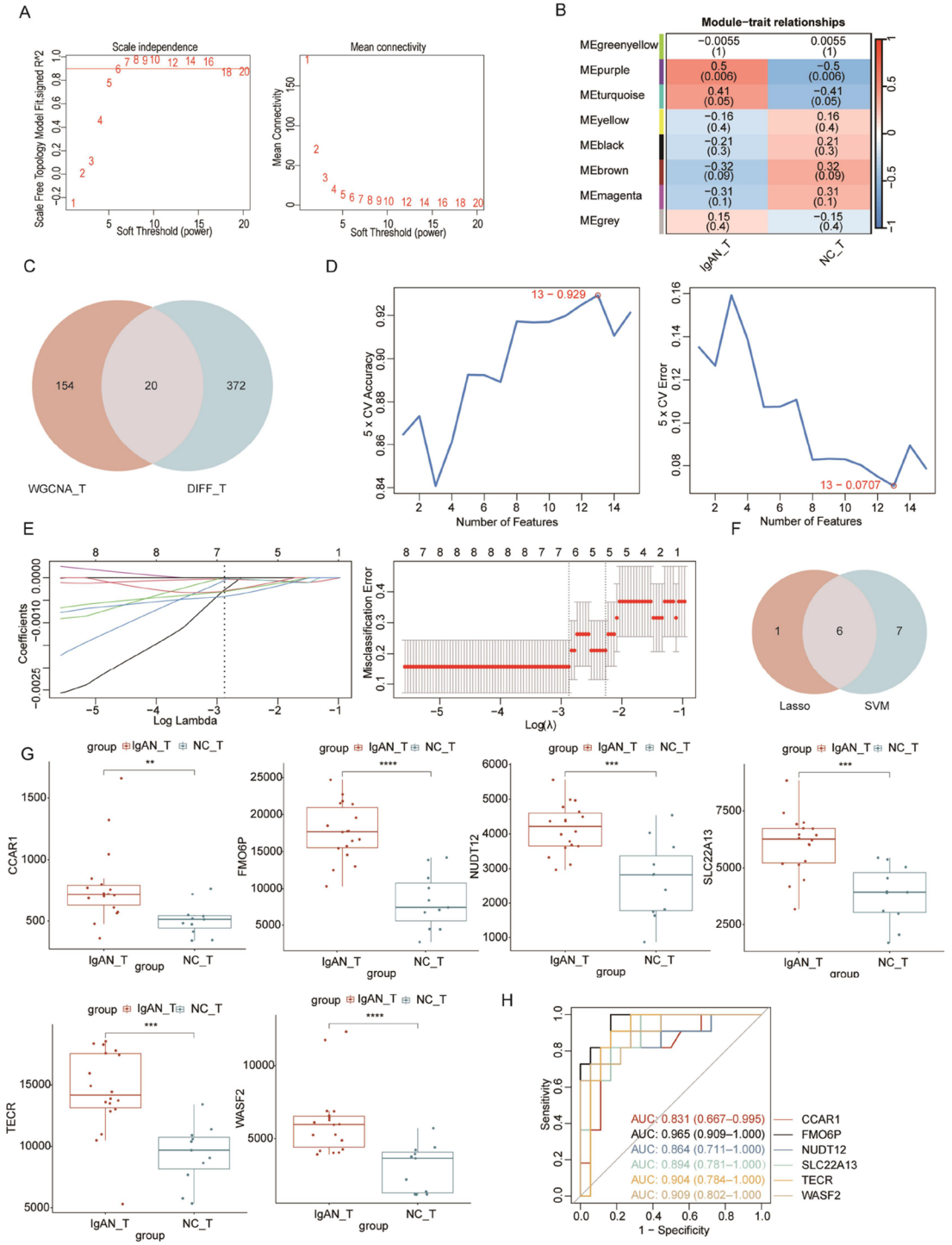


**Figure 4.** Screening of diagnostic markers by WGCNA and machine learning in tubules. (A) Analysis of the network topology for various soft threshold values. (B) Relationship between modules and clinical traits. The colors represent the correlation coefficients. (C) Venn diagram of key module proteins and DEPs. (D) Screening of biomarkers using the SVM-RFE algorithm. (E) LASSO logistic regression algorithm to identify diagnostic markers. (F) Venn diagram showing the overlap of diagnostic markers identified by both algorithms. (G) Boxplot illustrating the expression levels of hub genes between the IgAN group and the control group. *$p < 0.05$, **$p < 0.01$, ***$p < 0.001$, ****$p < 0.0001$. (H) ROC curve with AUC and 95%CI demonstrating the diagnostic efficacy of the identified biomarkers.

behaviors across the NC, IgAN II, IgAN III, and IgAN IV groups in the renal tubules. These profiles are identified as numbers 8, 11, 23, and 25 in Figure 7A. We also identified four significant protein profiles with different expression behaviors across the NC, IgAN II, IgAN III and IgAN IV groups in the interstitium, including profiles 15, 21, 24, and 25 in Figure 7B. Subsequently, by employing a Venn diagram, we compared the overlapping elements of profile 25 in both the tubular and interstitial regions (Figure 7C), and we were able to screen 41 overlapping proteins that increased with an increase in Lee's pathological grades, suggesting a positive correlation. To investigate the association between protein expression levels and clinical features, we



https://doi.org/10.1021/acsomega.4c07827
ACS Omega 2025, 10, 17208−17220

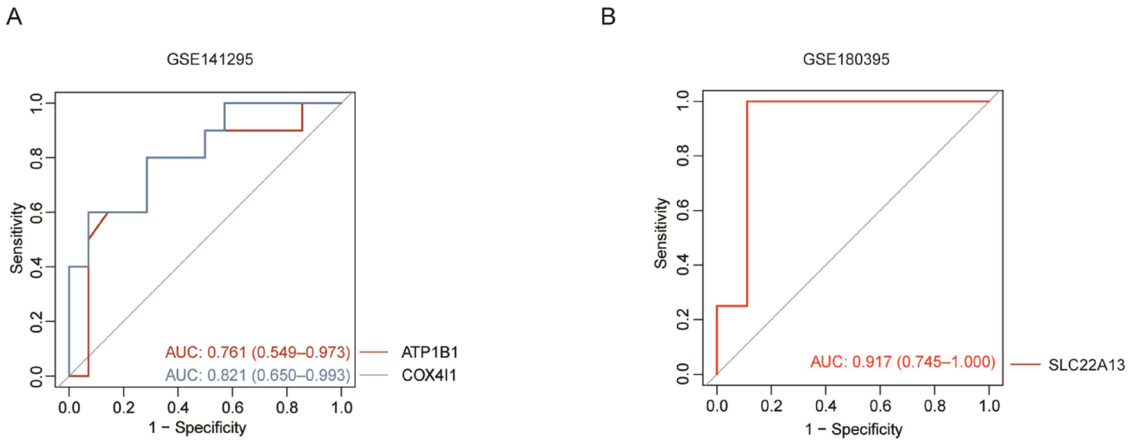


**Figure 5.** Diagnostic efficacy of the selected diagnostic markers for IgAN in the validation set. (A) ROC curve showing the AUC value and 95%CI of ATP1B1 and COX4I1, based on the dataset of the validation cohort in glomerulus. (B) ROC curve showing the AUC value and 95%CI of SLC22A13 based on the dataset of the validation cohort in tubules.

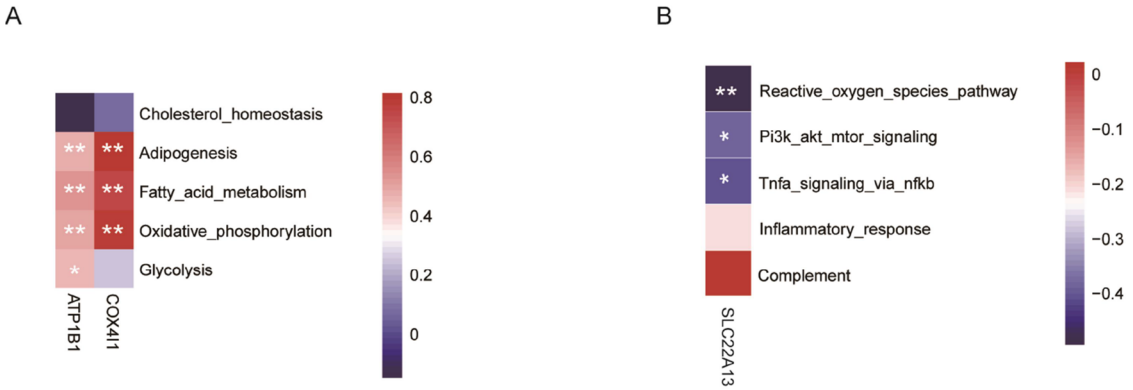


**Figure 6.** Pearson correlation analysis between hub proteins and GSVA: (A) glomerulus and (B) tubules. The colors represent the correlation coefficients. *$p < 0.05$, **$p < 0.01$.

conducted a correlation analysis. This analysis focused on the characteristics of protein expression and the key clinical features of proteinuria in IgAN patients. We found a total of 2 proteins (APEX1 and C4A) that were positively correlated to proteinuria (Figure 7D). The proteins in profile 25 were significantly enriched in ECM organizatin, actin filament-base movement, and coronavirus disease-COVID-19 on the Metascape platform in Figure7E.

## 3. DISCUSSION

In previous studies of renal proteomics, the focus was primarily on the analysis of whole tissues. However, these approaches provide limited insights into the specific dysfunctions affecting different compartments of the kidney. Considering that different compartments in IgAN may be associated with the activation of distinct signaling pathways, a more detailed understanding is necessary but has been lacking in prior research.

In our study comparing IgAN groups with control groups, we identified several DEPs: a total of 112 proteins were upregulated and 74 were downregulated in the glomerulus. In the renal tubules, 266 proteins were upregulated and 126 were downregulated, whereas in the renal interstitium, 113 proteins were upregulated and 118 were downregulated. Interestingly, we found that only three DEPs existed in the three regions of kidney, which was the molecular basis for the different pathological mechanisms of each substructure. In the subsequent KEGG functional analysis, we found that there were significant metabolic disorders in all three regions of the kidney, which may be the main pathological mechanism of IgAN. However, we found significant differences in the three substructures; for example, we found almost no immune dysfunction in the glomeruli and no fatty acid metabolism disorder in the renal interstitium. However, compared with other regions, the fatty acid synthesis in the glomeruli was its unique pathway, and the complement and coagulation cascades in the renal tubules were its unique pathway. However, since our subsequent analysis was based on DEPs screened for FC 1.5, we can only assume that fatty acid synthesis is more prominent in the pathological mechanism of the glomerulus than other substructures. Activation of complement and coagulation cascades is more pronounced in renal tubules. Based on these DEPs, we employed WGCNA and machine learning to screen for and identify diagnostic biomarkers for IgAN. Ultimately, we identified and validated two biomarkers in the glomerulus: ATP1B1 and COX4I1. Similarly, we identified and validated one biomarker in the renal tubules: SLC22A13. Furthermore, we utilized STEM to select biomarkers correlated with the severity of IgAN and found that C4A and APEX1 levels increased with the elevation of proteinuria.

Changes in lipid metabolism have been identified as a risk factor for the progression of CKD.[46] Fatty acids are established as a source of energy for various cells, including cardiac and muscular cells, and are known to facilitate cell proliferation and


https://doi.org/10.1021/acsomega.4c07827
ACS Omega 2025, 10, 17208−17220

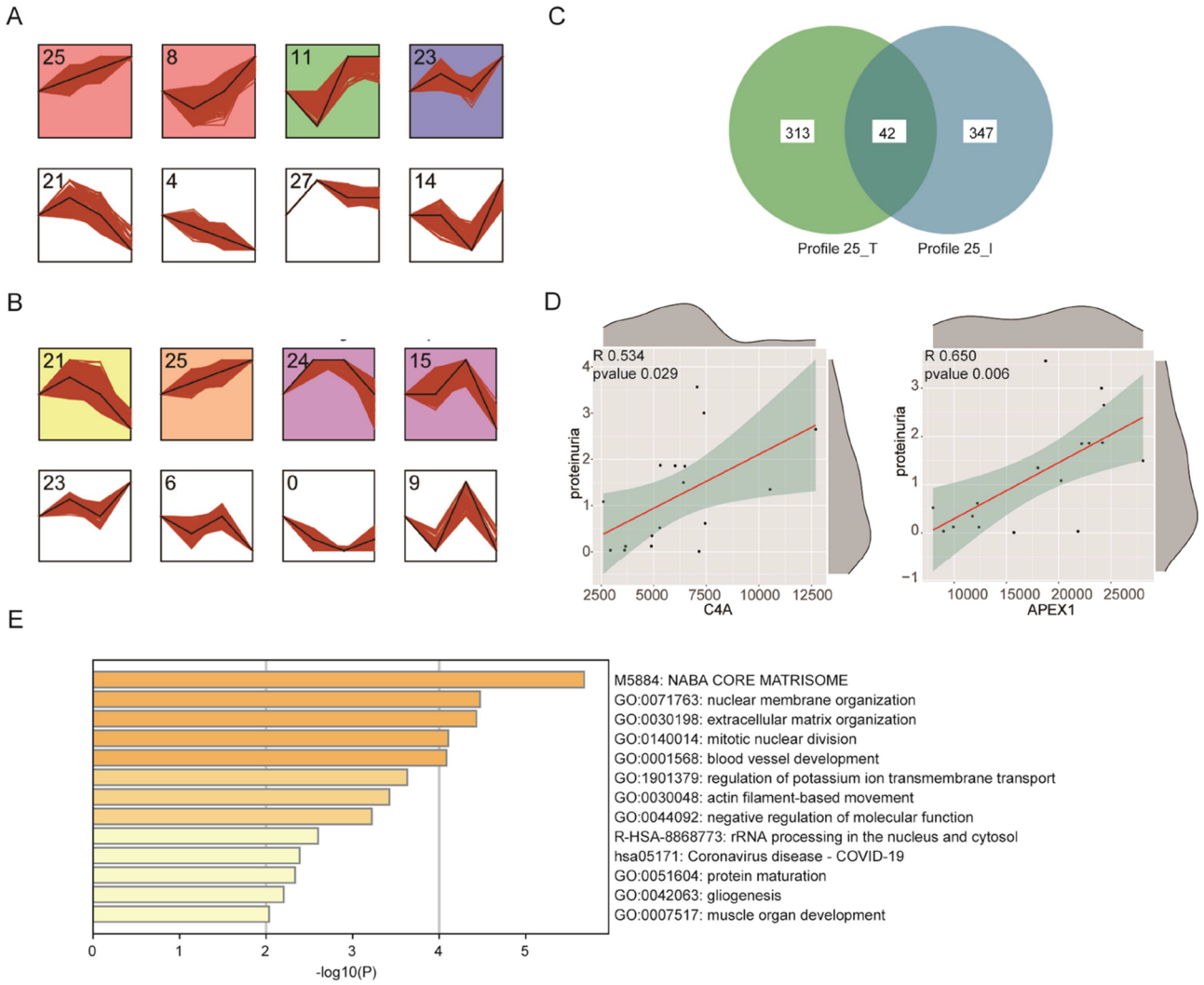


**Figure 7.** Proteomic profiles of STEM analysis for IgAN exacerbation. STEM analysis was applied to obtain the protein expression profiles across NC, IgAN II, IgAN III, and IgAN IV. The profile ID is shown at the top left corner of the profile: (A) tubules and (B) interstitium. (C) Venn diagram of profile 25 in the tubules and interstitium. (D) Correlation analysis of upregulated proteins and corresponding clinical characteristics of proteinuria to identify the exacerbation proteins. (E) Function analysis of profile 25 in the tubules and interstitium in Metascape platform ($P < 0.05$).

inflammation. The accumulation of lipids can induce inflammatory responses through the activation of unfolded proteins in the endoplasmic reticulum (ER), leading to ER stress and maladaptive responses. Furthermore, the activation of the unfolded protein response in the ER itself can trigger inflammation.[47,48] Experiments have shown that markers of ER stress have been detected in the glomerular endothelial cells or podocytes of both human and mouse models with IgAN.[49] ATP1B1 is the main subunit of $Na^+$-$K^+$-ATPase, which works in conjunction with $Ca^{2+}$-ATPase genes in $Ca^{2+}$ cycling.[50] Research indicates that increased intracellular $Ca^{2+}$ can stimulate lipolysis and thermogenesis in cells by triggering cAMP-mediated pathways.[51] Therefore, we speculate that in glomerular cells, the activation of Na/K-ATPase increases extracellular sodium ions, promoting $Na^+$−$Ca^{2+}$ exchange along the concentration gradient, thereby reducing the intracellular calcium ion concentration. This reduction in calcium ions inhibits cAMP-mediated pathways, leading to lipid accumulation. Enzymes involved in fatty acid metabolism produce crotonyl-CoA to facilitate lysine crotonylation; however, the absence of this modification can impair the expression of Cox4i1, leading to cellular dysfunction and promoting kidney damage and apoptosis.[52]

Currently, the prevailing explanation for the immunopathogenesis of IgAN is the "multi-hit" hypothesis.[2,53,54] Both genetic and environmental factors play a significant role.[54] Specifically, the immunopathogenesis of IgAN under the "multi-hit" hypothesis can be described as follows: The first hit involves the production of abnormally glycosylated IgA1. The second hit occurs when antibodies in circulation recognize these self-antigens. The third hit is the formation of pathogenic immune complexes containing IgA1 through the immune recognition. The fourth hit involves the deposition of these immune complexes in the glomerular mesangial areas, which then activates mesangial cells, stimulates cytokine secretion, and activates the complement system, leading to kidney damage.[2,53] IgAN is classified as an autoimmune disorder, where dysregulation and activation of the complement system are believed to be crucial factors contributing to renal injury in IgAN cases.[55] Our study found that the complement and coagulation pathways were abnormally activated in the renal tubules. Studies suggest that proximal tubular epithelial cells inherently exhibit characteristics of innate immunity, and these cells are capable of


https://doi.org/10.1021/acsomega.4c07827
ACS Omega 2025, 10, 17208−17220

producing pro-inflammatory factors, chemokines, and complement components.[56] SLC22A13, solute carrier family 22 member 13, a highly expressed transporter protein in renal tubules, can be used as a diagnostic and prognostic marker for identifying cell renal cell carcinoma.[57,58] SLC22A13 is involved in the transport and elimination of tyrosine derivatives, such as catecholamines and histamines.[59] In the immune system, histamine is mainly involved in allergic and inflammatory responses and immune regulation and actively interferes with peripheral immune tolerance induced by regulatory T cells through H2R and H4R.[60] Histamine is regulated and the immunosuppressive function of Treg cells is improved by destroying SLC22A13.[59]

In renal tissue, the interstitium refers to the areas between the tubules outside of the glomerulus and blood vessels. It contains various cells, such as fibroblast-like cells, and components of the ECM.[61,62] The ECM in these regions provides a physical microenvironment for cell survival, assists in cell anchoring, acts as a tissue scaffold, and also transmits signals from the surrounding environment to the cells.[63] Chronic progressive kidney damage is associated with changes in the renal interstitium, commonly referred to as interstitial fibrosis. This fibrosis is mainly caused by the accumulation of ECM, the proliferation of fibroblasts that can produce ECM, and the aggregation of monocytes.[61] Fibrosis involves the formation and accumulation of ECM and is closely associated with tissue regeneration and inflammation.[64] Interstitial fibrosis is associated with the extensive accumulation of ECM components in the interstitium and is directly related to the progression of kidney diseases.[65] This indicates that ECM−receptor interactions are a major factor in the renal interstitial lesions of IgAN.

We further identified C4A and APEX1 as biomarkers associated with the severity of proteinuria. These biomarkers may serve as important indicators for assessing the prognosis of IgAN patients and have a potential clinical application value. Complement C4-A (C4A) represents a pivotal molecule within the complement system and is a major constituent of the innate immune response. It possesses the ability to rapidly identify and neutralize invading microbes, thereby playing an essential role in the operation of the classical (CP) and lectin (LP) complement pathways.[66] In cases of IgAN, the presence of C4A is correlated with the severity of proteinuria.[67] This is consistent with our research findings. APEX1 plays a pivotal role in regulating cellular responses to oxidative stress, controlling the pace of cell proliferation, and preserving genomic stability.[68] Evidence indicates that the aberrant expression, post-translational modification, and subcellular relocation of the APE1 protein within renal tubular epithelial cells can initiate intracellular generation of reactive oxygen species (ROS) and apoptotic processes.[69] Although there is no direct evidence linking APEX1 to proteinuria, the detrimental effects of APEX1 in renal tubules may be a critical factor influencing the prognosis of the disease.

This study reveals the activation of distinct tissue-specific pathways and their key proteins in IgAN, providing important insights into the mechanisms of the disease and potential new therapeutic targets.

However, here, we need to specifically emphasize that we performed principal component analysis (PCA) to evaluate the overall variability among different compartments (glomeruli, tubules, and interstitium) in IgAN and healthy control samples. There was significant overlap between groups, with the total explained variance of the first two principal components being less than 15%. This result suggests a relatively low intergroup variability. However, this phenomenon may not fully reflect the underlying biological characteristics but could be influenced by other factors. Additionally, we calculated the coefficient of variation (CV) for each compartment and condition. The CV values indicate higher variability within certain groups, such as IgAN tubules and the interstitium. This increased variability is likely due to our samples being submitted for analysis in multiple batches, which could be the main reason for the elevated intragroup variability. High CV values suggest substantial variability among samples within the same group. Such intragroup variations may obscure intergroup differences, making it challenging for PCA to effectively differentiate between groups. Although the PCA results indicate low intergroup differences, this outcome could result from a combination of biological characteristics and technical factors. To further explore intergroup differences, we integrated CV analysis with subsequent differential expression analysis, focusing on identifying DEPs that remain consistent despite the high CV background. This approach effectively reduces the impact of technical variability and facilitates the identification of key proteins with potential biological significance.

In this study, we used transcriptomic datasets (GSE141295 and GSE180395) to validate key biomarkers identified through proteomic analysis. Although the correlation between mRNA and protein levels may be influenced by post-transcriptional regulation, translation efficiency, and protein degradation, transcriptomic data remain a common strategy for supporting findings from proteomic studies. Previous research has shown that while mRNA and protein levels do not always exhibit a one-to-one correlation, transcriptional changes in key disease-related genes can often reflect trends in protein expression. Therefore, in the absence of paired proteomic data, cross-validation using transcriptomic data can still provide some support for the reliability of potential biomarkers. Future studies will validate these biomarkers at the protein level in independent patient cohorts. Additionally, experimental validation methods such as Western blot or ELISA could further confirm their roles in the disease.

## 4. METHODS

**4.1. Patients.** This study included a cohort of 18 patients who were newly diagnosed with IgAN based on renal biopsy pathology conducted at the First Affiliated Hospital of Jinan University in Guangzhou, China. According to the grading system proposed by Lee et al., five patients were categorized as Grade II, eight as Grade III, and five as Grade IV.[70,71] None of these patients exhibited clinical or serological indications of autoimmune disorders, Henoch−Schönlein purpura, liver disease, or malignancy. In addition, 11 patients whose para-carcinoma tissue showed normal renal biopsy findings under light microscopy were selected as control subjects. A representative histopathological image of the kidney biopsy in the IgAN group is shown in Figure S2A, and that in the control group is shown in Figure S2B. Every participant signed informed consent before being included in the study. The study received approval from the ethics committee of the First Affiliated Hospital of Jinan University in Guangzhou, China (Reference no. KY-2020-034), which was carried out in accordance with the most recent edition of the Declaration of Helsinki.

**4.2. Specimen Preparation and LCM.** Each formalin-fixed, paraffin-embedded kidney tissue sample was sectioned by using a pathological slicer, resulting in tissue slices with a thickness of 10 $\mu$m. Subsequently, these slices were transferred


https://doi.org/10.1021/acsomega.4c07827
ACS Omega 2025, 10, 17208−17220

onto specially prepared frame film glass slides (PET frameslides, No. 11505190, Leica Microsystems, Germany) designated for LCM. The process then involved dewaxing, drying, and performing LCMs on the prepared tissue sections. A total of 86 renal substructure samples were obtained from the IgAN group and the NC group, including 18 glomerulus, 18 tubules, and 18 interstitium samples in the IgAN group, and 11 glomerulus, 11 tubules, and 10 interstitium samples in the normal group. The representative images of renal tissue regions (the glomerulus, tubules, and renal interstitium) before and after microincision on the frame film slide are shown in Figure S3A.

**4.3. Data Acquisition.** We proceeded to extract protein from the tissue slices followed by enzymatic digestion and desalting. The specific process for protein extraction was as follows:[1] The sample tubes containing an appropriate amount of tissue samples were placed in a centrifuge and centrifuged for 10 min.[2] 20 $\mu$L of a 10 mM DTT solution was added to 50 mM ammonium bicarbonate.[3] The reaction was carried out in a 95°C metal bath for 30 min.[4] After the temperature returned to room temperature, IAM was immediately added to a final concentration of 50 mM, and the mixture was left in the dark at room temperature for 30 min.[5] Finally, the sample tubes were placed in an ultrasonic instrument and sonicated for 20 min. Subsequently, the peptides separated by the liquid-phase system were transferred to a series of mass spectrometers for detection in the DDA and DIA modes. The DDA data were processed and identified by using MaxQuant software (version 1.5.3.30). For the analysis of DIA data, we utilized Spectronaut (version 12), employing indexed retention time (iRT) peptides for the calibration of retention time.[72]

**4.4. Identification of Differential Protein Expression.** After processing with MSstats software (Version 4.0), the protein scale was generated, and then it was used for Quantile normalization. PCA is a dimensionality reduction method and an orthogonal transformation of correlated variables into a set of linearly uncorrelated variables. It is primarily used to observe separation trends between groups and identify outliers, reflecting intergroup and intragroup variability based on the original data. The intragroup CV and PCA for this study are shown in Figure S4. Following this, we utilized the Limma package (Version 3.56.2) in R to identify proteins that exhibited significantly altered expression levels between the IgAN and control groups. These DEPs were defined by a statistical significance threshold of $P < 0.05$ and a fold change greater than 1.5.

**4.5. Enrichment Analysis.** DEPs (including upregulated and downregulated) were analyzed using GO and KEGG analyses, facilitated by the clusterProfiler package (Version 4.8.3) in R.[73] A cutoff criterion of $p < 0.05$ was used to indicate significant differences in the GO and KEGG pathways. In our study, we performed GSEA to identify the most significant functional items between IgAN and controls. For the analysis, we selected the gene set "c2.cp.kegg.v7.0.symbols.gmt" from the Molecular Signatures Database (MSigDB) as the reference gene set. We considered gene sets with a net enrichment score (NES) $|NES| > 1.5$ and a $p$-value $< 0.05$ as significantly enriched, which was our threshold for identifying key pathways involved in IgAN.

**4.6. WGCNA to Identify Networks of Co-Expressed DEPs.** Utilizing the WGCNA package (Version 1.72_1) in R, proteins were grouped into distinct modules. In summary, this process involved the identification and weighting of connections between protein pairs, which was determined by their correlated expression levels across multiple samples. Subsequently, we transformed the adjacency matrix into a topological overlap matrix (TOM) to evaluate the connectivity among genes within the network. Hierarchical clustering was then applied to detect clusters (modules) of genes that exhibited high interconnectedness based on their connectivity and covariance coefficients. The minimum size for the gene dendrogram was set at 25. We selected an appropriate soft-thresholding power to define a substantial positive correlation among genes within each module. Furthermore, we gathered relevant proteomic information related to the selected module to facilitate a subsequent in-depth analysis.

**4.7. Identification of Diagnostic Markers.** To screen for potential diagnostic markers for IgAN, we utilized two advanced algorithms: Least Absolute Shrinkage and Selection Operator (LASSO) logistic regression and Support Vector Machine-Recursive Feature Elimination (SVM-RFE). The LASSO logistic regression, implemented using the "glmnet" R package (ver. 4.1_8), is a regularization method that enhances the prediction accuracy and interpretability of the statistical model it creates. By applying a penalty proportional to the absolute value of the coefficients, LASSO effectively shrinks some coefficients to zero, thereby performing variable selection and identifying the most relevant diagnostic markers. On the other hand, SVM-RFE is a powerful feature selection technique that recursively eliminates the least significant features, ensuring that the optimal set of variables is retained for the model. This method ranks features based on their importance to the support the classification performance of the vector machine and iteratively removes the least important features to refine the model. By combining the outputs of these two algorithms, we selected the candidate diagnostic markers for further investigation.

**4.8. Verification of the Diagnostic Markers.** The uniformly expressed matrix files for IgAN glomeruli and renal tubule protein samples were downloaded from the GEO database (https://www.ncbi.nlm.nih.gov/geo/), specifically GSE141295 (glomeruli: 14 IgAN cases, 10 healthy controls) and GSE180395 (renal tubules: 4 IgAN cases, 9 healthy controls) as validation sets. To evaluate the diagnostic performance of the candidate markers, ROC curves were plotted based on the validation datasets.

**4.9. GSVA and Pearson Correlation Analysis.** Initially, the raw expression matrix was standardized to ensure data quality. Subsequently, pathway enrichment analysis was conducted using the "GSVA" package (ver. 4.48.3), which identifies functionally related biological pathways by assessing variations in gene set expressions. Following this, Pearson correlation analysis was performed using the "corr.test()" function from the "psych" package (ver. 4.4.6.26) to evaluate the relationships between key proteins and pathway enrichment scores. Throughout this process, a $p$-value of less than 0.05 was used as the criterion for determining significant correlations.

**4.10. Short Time-Series Expression Minor Analysis.** To identify molecular signatures associated with the progression of IgAN, we utilized the STEM analysis (http://sb.cs.cmu.edu/stem) to classify protein expression profiles derived from healthy controls and IgAN stages II, III, and IV. Prior to analysis, the expression data were subjected to normalization, and the STEM clustering method was applied. We established a minimum absolute expression change of 0.5 as a filter for molecular selection and limited the correlation threshold between any two model profiles to 0.9. Profiles with a $p$-value $< 0.05$, determined based on the number of clustered genes, were considered as significantly enriched clusters.



https://doi.org/10.1021/acsomega.4c07827
ACS Omega 2025, 10, 17208−17220

**4.11. Functional Enrichment Analysis for Profile 25 by Metascape.** To analyze the proteins within profile 25 from both the tubules and interstitium, we conducted pathway enrichment analysis using Metascape (https://metascape.org). For this analysis, we configured specific parameters, including a minimum overlap of 3 and a *p*-value cutoff of 0.05.

**4.12. Statistical Analyses.** All statistical analyses in our study were performed by using R software (version 4.3.1). The collected clinical data were expressed by mean ± standard deviation. We defined proteins as differentially expressed if they met the criteria of a p-value less than 0.05 and an FC greater than 1.5 or less than 0.67. The relationships between clinical parameters and proteins were quantified using Spearman's correlation. To assess statistical significance, we employed a range of tests selected based on their appropriateness for the specific data characteristics: unpaired two-tailed Student's t-test, Mann−Whitney U test, moderated t-test, permutation test, likelihood-ratio test, or Wilcoxon rank-sum test. The choice of test was determined by the distribution and properties of the data being analyzed.

## 5. CONCLUSIONS

This study revealed the activation of tissue-specific pathways and key proteins in IgAN, providing important insights into the mechanisms of the disease and the therapeutic potential. Additionally, diagnostic biomarkers were identified through machine-learning methods, offering valuable perspectives for the future noninvasive diagnosis of IgAN. However, this study has several limitations. First, the sample size was not large enough. Furthermore, the validation of potential biomarkers was performed solely using database-based data. For a deeper understanding of the pathogenic mechanisms in different IgAN substructures, developing a method to calculate their scores within specific pathogenic mechanisms would more intuitively reflect the focus of different substructures on certain disease processes.

## ■ ASSOCIATED CONTENT

### Data Availability Statement

The raw data for the health group is accessible in the CNGBdb repository. The accession number is CNP0004014, but the raw data for disease group will be accessible from the corresponding authors upon request.

### Supporting Information

The Supporting Information is available free of charge at https://pubs.acs.org/doi/10.1021/acsomega.4c07827.

Clinical information on the patients; a list of DEPs, KEGG pathway enrichment results, and a list of abbreviations used in the manuscript (XLSX)

Supplementary figures related to the experimental data (PDF)

## ■ AUTHOR INFORMATION


### Corresponding Authors

**Lianghong Yin** − *Institute of Kidney Disease and Blood Purification, The First Affiliated Hospital of Jinan University, Guangzhou 510630, China;* orcid.org/0000-0002-5005-5304; Email: yin-yun@126.com

**Donge Tang** − *Clinical Medical Research Center, The Second Clinical Medical College, Jinan University, Shenzhen People' s Hospital, Shenzhen 518020, China;* orcid.org/0000-0001-7011-196X; Email: donge66@126.com

**Yong Dai** − *Clinical Medical Research Center, The Second Clinical Medical College, Jinan University, Shenzhen People' s Hospital, Shenzhen 518020, China; Department of Organ Transplantation, The 924th Hospital of the Chinese People's Liberation Army Joint Logistic Support Force, Guilin 541002, China; School of Medicine, The First Affiliated Hospital, Anhui University of Science and Technology, Huainan 232001, China;* orcid.org/0000-0002-6840-9158; Email: daiyong22@aliyun.com

### Authors

**Jingxian Huang** − *Institute of Kidney Disease and Blood Purification, The First Affiliated Hospital of Jinan University, Guangzhou 510630, China;* orcid.org/0009-0002-1562-2032

**Hongguo Zhu** − *Institute of Kidney Disease and Blood Purification, The First Affiliated Hospital of Jinan University, Guangzhou 510630, China; Comprehensive Health Industry Research Center, Taizhou Research Institute, Southern University of Science and Technology, Taizhou 317000, China*

**Shanshan Li** − *Clinical Medical Research Center, The Second Clinical Medical College, Jinan University, Shenzhen People' s Hospital, Shenzhen 518020, China*

**Jing Qiu** − *Clinical Medical Research Center, The Second Clinical Medical College, Jinan University, Shenzhen People' s Hospital, Shenzhen 518020, China*

**Hougang Yang** − *Comprehensive Health Industry Research Center, Taizhou Research Institute, Southern University of Science and Technology, Taizhou 317000, China*

**Fengping Zheng** − *Institute of Kidney Disease and Blood Purification, The First Affiliated Hospital of Jinan University, Guangzhou 510630, China; Department of Organ Transplantation, The 924th Hospital of the Chinese People's Liberation Army Joint Logistic Support Force, Guilin 541002, China;* orcid.org/0000-0002-6065-3500

**Zhifeng Luo** − *Institute of Kidney Disease and Blood Purification, The First Affiliated Hospital of Jinan University, Guangzhou 510630, China; Department of Organ Transplantation, The 924th Hospital of the Chinese People's Liberation Army Joint Logistic Support Force, Guilin 541002, China*

**Qiang Yan** − *Department of Organ Transplantation, The 924th Hospital of the Chinese People's Liberation Army Joint Logistic Support Force, Guilin 541002, China*

**Fanna Liu** − *Institute of Kidney Disease and Blood Purification, The First Affiliated Hospital of Jinan University, Guangzhou 510630, China*

Complete contact information is available at: https://pubs.acs.org/10.1021/acsomega.4c07827


### Author Contributions

#J.H., H.Z., and S.L. contributed equally to this work and should be considered co-first authors.

### Author Contributions

Project administration, J.H., H.Z.; conceptualization, J.H.; funding acquisition, Y.D., D.T., L.Y.; writing—original draft, J.H.; methodology, H.Y.; visualization, S.L., H.Z.; editing, J.Q.; data collation, F.Z.; formal analysis, Z.L., Q.Y.; resources, F.L.; supervision, J.H., H.Z.

### Notes

The authors declare no competing financial interest.

## ■ ACKNOWLEDGMENTS

This work was supported by the Guangzhou Entrepreneurship Leading Team (No. 202009030005), the Shenzhen Science and Technology Program (Nos. GJHZ20220913142614027 and JCYJ20210324113214039), and the Taizhou Science and Technology Plan Project (No. 23ywa60). In addition, we thank Qi Yin from BGI Genomics for his assistance in uploading our data to the public database.

## ■ REFERENCES

(1) Berthoux, FC; Mohey, H.; Afiani, A. Natural history of primary IgA nephropathy. *Semin Nephrol* **2008**, *28*, 4−9.
(2) Lai, KN; Tang, SC; Schena, FP; Novak, J.; Tomino, Y.; Fogo, AB; Glassock, RJ *IgA nephropathy. Nat. Rev. Dis Primers* **2016**, *2*, 16001.
(3) Novak, J.; Julian, BA; Mestecky, J.; Renfrow, MB Glycosylation of IgA1 and pathogenesis of IgA nephropathy. *Semin Immunopathol* **2012**, *34*, 365−382.
(4) Cheung, CK; Barratt, J. Biomarkers to Predict Progression in IgA Nephropathy. *Clin J. Am. Soc. Nephrol* **2019**, *14*, 1421−1423.
(5) Magistroni, R.; D'Agati, VD; Appel, GB; Kiryluk, K. New developments in the genetics, pathogenesis, and therapy of IgA nephropathy. *Kidney Int.* **2015**, *88*, 974−989.
(6) Floege, J.; Amann, K. Primary glomerulonephritides. *Lancet* **2016**, *387*, 2036−2048.
(7) McGrogan, A.; Franssen, CF; de Vries, CS The incidence of primary glomerulonephritis worldwide: a systematic review of the literature. *Nephrol Dial Transplant* **2011**, *26*, 414−430.
(8) Mestecky, J.; Novak, J.; Moldoveanu, Z.; Raska, M. IgA nephropathy enigma. *Clin Immunol* **2016**, *172*, 72−77.
(9) Li, LS; Liu, ZH Epidemiologic data of renal diseases from a single unit in China: analysis based on 13,519 renal biopsies. *Kidney Int.* **2004**, *66*, 920−923.
(10) van der Boog, PJ.; van Kooten, C.; de Fijter, JW; Daha, MR Role of macromolecular IgA in IgA nephropathy. *Kidney Int.* **2005**, *67*, 813−821.
(11) Kiryluk, K.; Novak, J.; Gharavi, AG Pathogenesis of immunoglobulin A nephropathy: recent insight from genetic studies. *Annu. Rev. Med.* **2013**, *64*, 339−356.
(12) Kiryluk, K.; Li, Y.; Scolari, F.; Sanna-Cherchi, S.; Choi, M.; Verbitsky, M.; Fasel, D.; Lata, S.; Prakash, S.; Shapiro, S.; et al. Discovery of new risk loci for IgA nephropathy implicates genes involved in immunity against intestinal pathogens. *Nat. Genet* **2014**, *46*, 1187−1196.
(13) Knoppova, B.; Reily, C.; Maillard, N.; Rizk, DV; Moldoveanu, Z.; Mestecky, J.; Raska, M.; Renfrow, MB; Julian, BA; Novak, J. The Origin and Activities of IgA1-Containing Immune Complexes in IgA Nephropathy. *Front Immunol* **2016**, *7*, 117.
(14) D'Amico, G. Natural history of idiopathic IgA nephropathy: role of clinical and histological prognostic factors. *Am. J. Kidney Dis* **2000**, *36*, 227−237.
(15) Shi, M.; Ouyang, Y.; Yang, M.; Yang, M.; Zhang, X.; Huang, W.; Wang, W.; Wang, Z.; Zhang, W.; Chen, X.; et al. IgA Nephropathy Susceptibility Loci and Disease Progression. *Clin J. Am. Soc. Nephrol* **2018**, *13*, 1330−1338.
(16) Robert, T.; Berthelot, L.; Cambier, A.; Rondeau, E.; Monteiro, RC Molecular Insights into the Pathogenesis of IgA Nephropathy. *Trends Mol. Med.* **2015**, *21*, 762−775.
(17) Zhang, C.; Zeng, X.; Li, Z.; Wang, Z.; Li, S. Immunoglobulin A nephropathy: current progress and future directions. *Transl Res.* **2015**, *166*, 134−144.
(18) Makita, Y.; Suzuki, H.; Kano, T.; Takahata, A.; Julian, BA; Novak, J.; Suzuki, Y. TLR9 activation induces aberrant IgA glycosylation via APRIL- and IL-6-mediated pathways in IgA nephropathy. *Kidney Int.* **2020**, *97*, 340−349.
(19) Espina, V.; Wulfkuhle, JD; Calvert, VS; VanMeter, A.; Zhou, W.; Coukos, G.; Geho, DH; Petricoin, EF, 3rd; Liotta, LA Laser-capture microdissection. *Nat. Protoc* **2006**, *1*, 586−603.
(20) Burgemeister, R. Laser capture microdissection of FFPE tissue sections bridging the gap between microscopy and molecular analysis. *Methods Mol. Biol.* **2011**, *724*, 105−115.
(21) Aebersold, R.; Mann, M. Mass spectrometry-based proteomics. *Nature* **2003**, *422*, 198−207.
(22) Qian, WJ; Jacobs, JM; Liu, T.; Camp, DG, 2nd; Smith, RD Advances and challenges in liquid chromatography-mass spectrometry-based proteomics profiling for clinical applications. *Mol. Cell Proteomics* **2006**, *5*, 1727−1744.
(23) Gillet, LC; Navarro, P.; Tate, S.; Röst, H.; Selevsek, N.; Reiter, L.; Bonner, R.; Aebersold, R. Targeted data extraction of the MS/MS spectra generated by data-independent acquisition: a new concept for consistent and accurate proteome analysis. *Mol. Cell. Proteomics* **2012**, *11*, O111.016717.
(24) Liu, Y.; Hüttenhain, R.; Surinova, S.; Gillet, LC; Mouritsen, J.; Brunner, R.; Navarro, P.; Aebersold, R. Quantitative measurements of N-linked glycoproteins in human plasma by SWATH-MS. *Proteomics* **2013**, *13*, 1247−1256.
(25) Schubert, OT; Gillet, LC; Collins, BC; Navarro, P.; Rosenberger, G.; Wolski, WE; Lam, H.; Amodei, D.; Mallick, P.; MacLean, B.; Aebersold, R. Building high-quality assay libraries for targeted analysis of SWATH MS data. *Nat. Protoc* **2015**, *10*, 426−441.
(26) Röst, HL; Liu, Y.; D'Agostino, G.; Zanella, M.; Navarro, P.; Rosenberger, G.; Collins, BC; Gillet, L.; Testa, G.; Malmström, L.; Aebersold, R. TRIC: an automated alignment strategy for reproducible protein quantification in targeted proteomics. *Nat. Methods* **2016**, *13*, 777−783.
(27) Ludwig, C.; Gillet, L.; Rosenberger, G.; Amon, S.; Collins, BC; Aebersold, R. Data-independent acquisition-based SWATH-MS for quantitative proteomics: a tutorial. *Mol. Syst. Biol.* **2018**, *14*, No. e8126.
(28) Collins, BC; Hunter, CL; Liu, Y.; Schilling, B.; Rosenberger, G.; Bader, SL; Chan, DW; Gibson, BW; Gingras, AC; Held, JM; et al. Multi-laboratory assessment of reproducibility, qualitative and quantitative performance of SWATH-mass spectrometry. *Nat. Commun.* **2017**, *8*, 291.
(29) Midha, MK; Kusebauch, U.; Shteynberg, D.; Kapil, C.; Bader, SL; Reddy, PJ.; Campbell, DS; Baliga, NS; Moritz, RL A comprehensive spectral assay library to quantify the Escherichia coli proteome by DIA/SWATH-MS. *Sci. Data* **2020**, *7*, 389.
(30) Krasny, L.; Huang, PH Data-independent acquisition mass spectrometry (DIA-MS) for proteomic applications in oncology. *Mol. Omics* **2021**, *17*, 29−42.
(31) Liu, Y.; Buil, A.; Collins, BC; Gillet, LC; Blum, LC; Cheng, LY; Vitek, O.; Mouritsen, J.; Lachance, G.; Spector, TD; et al. Quantitative variability of 342 plasma proteins in a human twin population. *Mol. Syst. Biol.* **2015**, *11*, 786.
(32) Schubert, OT; Ludwig, C.; Kogadeeva, M.; Zimmermann, M.; Rosenberger, G.; Gengenbacher, M.; Gillet, LC; Collins, BC; Röst, HL; Kaufmann, SH; et al. Absolute Proteome Composition and Dynamics during Dormancy and Resuscitation of Mycobacterium tuberculosis. *Cell Host Microbe* **2015**, *18*, 96−108.
(33) Guo, T.; Kouvonen, P.; Koh, CC; Gillet, LC; Wolski, WE; Röst, HL; Rosenberger, G.; Collins, BC; Blum, LC; Gillessen, S.; et al. Rapid mass spectrometric conversion of tissue biopsy samples into permanent quantitative digital proteome maps. *Nat. Med.* **2015**, *21*, 407−413.
(34) Nakatani, S.; Wei, M.; Ishimura, E.; Kakehashi, A.; Mori, K.; Nishizawa, Y.; Inaba, M.; Wanibuchi, H. Proteome analysis of laser microdissected glomeruli from formalin-fixed paraffin-embedded kidneys of autopsies of diabetic patients: nephronectin is associated with the development of diabetic glomerulosclerosis. *Nephrol Dial Transplant* **2012**, *27*, 1889−1897.
(35) Ning, X.; Yin, Z.; Li, Z.; Xu, J.; Wang, L.; Shen, W.; Lu, Y.; Cai, G.; Zhang, X.; Chen, X. Comparative proteomic analysis of urine and laser microdissected glomeruli in IgA nephropathy. *Clin Exp Pharmacol Physiol* **2017**, *44*, 576−585.
(36) Sethi, S.; Madden, BJ; Debiec, H.; Charlesworth, MC; Gross, L.; Ravindran, A.; Hummel, AM; Specks, U.; Fervenza, FC; Ronco, P. Exostosin 1/Exostosin 2-Associated Membranous Nephropathy. *J. Am. Soc. Nephrol* **2019**, *30*, 1123−1136.


https://doi.org/10.1021/acsomega.4c07827
*ACS Omega* 2025, 10, 17208−17220

(37) Sethi, S.; Debiec, H.; Madden, B.; Vivarelli, M.; Charlesworth, MC; Ravindran, A.; Gross, L.; Ulinski, T.; Buob, D.; Tran, CL; et al. Semaphorin 3B-associated membranous nephropathy is a distinct type of disease predominantly present in pediatric patients. *Kidney Int.* **2020**, *98*, 1253−1264.
(38) Sethi, S.; Vrana, JA; Theis, JD; Leung, N.; Sethi, A.; Nasr, SH; Fervenza, FC; Cornell, LD; Fidler, ME; Dogan, A. Laser microdissection and mass spectrometry-based proteomics aids the diagnosis and typing of renal amyloidosis. *Kidney Int.* **2012**, *82*, 226−234.
(39) Sethi, S.; Gamez, J. D.; Vrana, J. A.; Theis, J. D.; Bergen, H. R., 3rd; Zipfel, P. F.; Dogan, A.; Smith, R. J. H. Glomeruli of Dense Deposit Disease contain components of the alternative and terminal complement pathway. *Kidney Int.* **2009**, *75*, 952−960.
(40) Sethi, S.; Theis, JD; Vrana, JA; Fervenza, FC; Sethi, A.; Qian, Q.; Quint, P.; Leung, N.; Dogan, A.; Nasr, SH Laser microdissection and proteomic analysis of amyloidosis, cryoglobulinemic GN, fibrillary GN, and immunotactoid glomerulopathy. *Clin J. Am. Soc. Nephrol* **2013**, *8*, 915−921.
(41) Sethi, S.; Fervenza, FC; Zhang, Y.; Zand, L.; Vrana, JA; Nasr, SH; Theis, JD; Dogan, A.; Smith, RJ C3 glomerulonephritis: clinicopathological findings, complement abnormalities, glomerular proteomic profile, treatment, and follow-up. *Kidney Int.* **2012**, *82*, 465−473.
(42) Satoskar, AA; Shapiro, JP; Bott, CN; Song, H.; Nadasdy, GM; Brodsky, SV; Hebert, LA; Birmingham, DJ.; Nadasdy, T.; Freitas, MA; Rovin, BH Characterization of glomerular diseases using proteomic analysis of laser capture microdissected glomeruli. *Mod. Pathol* **2012**, *25*, 709−721.
(43) Han, X.; Yuan, T.; Zhang, J.; Shi, Y.; Li, D.; Dong, Y.; Fan, S. FOXO4 peptide targets myofibroblast ameliorates bleomycin-induced pulmonary fibrosis in mice through ECM-receptor interaction pathway. *J. Cell Mol. Med.* **2022**, *26*, 3269−3280.
(44) Yao, M.; Lian, D.; Wu, M.; Zhou, Y.; Fang, Y.; Zhang, S.; Zhang, W.; Yang, Y.; Li, R.; Chen, H.; et al. Isoliensinine Attenuates Renal Fibrosis and Inhibits TGF-$\beta$1/Smad2/3 Signaling Pathway in Spontaneously Hypertensive Rats. *Drug Des Devel Ther* **2023**, *17*, 2749−2762.
(45) Mohammadi Majd, T.; Kalantari, S.; Raeisi Shahraki, H.; Nafar, M.; Almasi, A.; Samavat, S.; Parvin, M.; Hashemian, A. Application of Sparse Linear Discriminant Analysis and Elastic Net for Diagnosis of IgA Nephropathy: Statistical and Biological Viewpoints. *Iran Biomed J.* **2018**, *22*, 374−384.
(46) Ruan, XZ.; Varghese, Z.; Moorhead, JF An update on the lipid nephrotoxicity hypothesis. *Nat. Rev. Nephrol* **2009**, *5*, 713−721.
(47) Gregor, MF; Hotamisligil, GS Inflammatory mechanisms in obesity. *Annu. Rev. Immunol* **2011**, *29*, 415−445.
(48) Hotamisligil, GS Inflammation, metaflammation and immunometabolic disorders. *Nature* **2017**, *542*, 177−185.
(49) Tanaka, M.; Moniwa, N.; Nogi, C.; Kano, T.; Matsumoto, M.; Sakai, A.; Maeda, T.; Takizawa, H.; Ogawa, Y.; Asanuma, K.; et al. Glomerular expression and urinary excretion of fatty acid-binding protein 4 in IgA nephropathy. *J. Nephrol* **2023**, *36*, 385−395.
(50) Aschauer, L.; Gruber, LN; Pfaller, W.; Limonciel, A.; Athersuch, TJ; Cavill, R.; Khan, A.; Gstraunthaler, G.; Grillari, J.; Grillari, R.; et al. Delineation of the key aspects in the regulation of epithelial monolayer formation. *Mol. Cell Biol.* **2013**, *33*, 2535−2550.
(51) Lan, Q.; Liufu, S.; Liu, X.; Ai, N.; Xu, X.; Li, X.; Yu, Z.; Yin, Y.; Liu, M.; Ma, H. Comprehensive analysis of transcriptomic and metabolomic profiles uncovered the age-induced dynamic development pattern of subcutaneous fat in Ningxiang pig. *Gene* **2023**, *880*, No. 147624.
(52) Li, Y.; Wang, Z.; Xu, H.; Hong, Y.; Shi, M.; Hu, B.; Wang, X.; Ma, S.; Wang, M.; Cao, C.; et al. Targeting the transmembrane cytokine co-receptor neuropilin-1 in distal tubules improves renal injury and fibrosis. *Nat. Commun.* **2024**, *15*, 5731.
(53) Suzuki, H.; Kiryluk, K.; Novak, J.; Moldoveanu, Z.; Herr, AB; Renfrow, MB; Wyatt, RJ.; Scolari, F.; Mestecky, J.; Gharavi, AG; Julian, BA The pathophysiology of IgA nephropathy. *J. Am. Soc. Nephrol* **2011**, *22*, 1795−1803.
(54) Penfold, RS; Prendecki, M.; McAdoo, S.; Tam, FW Primary IgA nephropathy: current challenges and future prospects. *Int. J. Nephrol Renovasc Dis* **2018**, *11*, 137−148.
(55) Tortajada, A.; Gutierrez, E.; Pickering, MC; Praga Terente, M.; Medjeral-Thomas, N. The role of complement in IgA nephropathy. *Mol. Immunol* **2019**, *114*, 123−132.
(56) Deng, Z.; Jing, Z.; Guo, Y.; Ma, J.; Yan, H.; Shi, Z.; Deng, H.; Liang, Y.; Wang, S.; Cui, Z.; et al. Expression of immunoglobulin G in human proximal tubular epithelial cells. *Mol. Med. Rep.* **2021**, *23*, 327.
(57) Kang, W.; Zhang, M.; Wang, Q.; Gu, D.; Huang, Z.; Wang, H.; Xiang, Y.; Xia, Q.; Cui, Z.; Jin, X. The SLC Family Are Candidate Diagnostic and Prognostic Biomarkers in Clear Cell Renal Cell Carcinoma. *Biomed Res. Int.* **2020**, *2020*, No. 1932948.
(58) Ohtsu, N.; Ohgaki, R.; Jin, C.; Xu, M.; Okanishi, H.; Takahashi, R.; Matsui, A.; Kishimoto, W.; Ishiguro, N.; Kanai, Y. Functional coupling of organic anion transporter OAT10 (SLC22A13) and monocarboxylate transporter MCT1 (SLC16A1) influencing the transport function of OAT10. *J. Pharmacol Sci.* **2022**, *150*, 41−48.
(59) Zhu, P.; Hata, R.; Ogasawara, M.; Cao, F.; Kameda, K.; Yamauchi, K.; Schinkel, AH; Maeyama, K.; Sakanaka, M. Targeted disruption of organic cation transporter 3 (Oct3) ameliorates ischemic brain damage through modulating histamine and regulatory T cells. *J. Cereb Blood Flow Metab* **2012**, *32*, 1897−1908.
(60) Jutel, M.; Akdis, M.; Akdis, CA Histamine, histamine receptors and their role in immune pathology. *Clin Exp Allergy* **2009**, *39*, 1786−1800.
(61) Zeisberg, M.; Kalluri, R. Physiology of the Renal Interstitium. *Clin J. Am. Soc. Nephrol* **2015**, *10*, 1831−1840.
(62) Lemley, KV; Kriz, W. Anatomy of the renal interstitium. *Kidney Int.* **1991**, *39*, 370−381.
(63) Geiger, B.; Bershadsky, A.; Pankov, R.; Yamada, KM Transmembrane crosstalk between the extracellular matrix−cytoskeleton crosstalk. *Nat. Rev. Mol. Cell Biol.* **2001**, *2*, 793−805.
(64) Djudjaj, S.; Boor, P. Cellular and molecular mechanisms of kidney fibrosis. *Mol. Aspects Med.* **2019**, *65*, 16−36.
(65) Meran, S.; Steadman, R. Fibroblasts and myofibroblasts in renal fibrosis. *Int. J. Exp Pathol* **2011**, *92*, 158−167.
(66) Wang, H.; Liu, M. Complement C4, Infections, and Autoimmune Diseases. *Front Immunol* **2021**, *12*, No. 694928.
(67) Genest, DS; Bonnefoy, A.; Khalili, M.; Merlen, C.; Genest, G.; Lapeyraque, AL; Patey, N.; Smail, N.; Royal, V.; Troyanov, S. Comparison of Complement Pathway Activation in Autoimmune Glomerulonephritis. *Kidney Int. Rep* **2022**, *7*, 1027−1036.
(68) Ataya, FS; Fouad, D.; Malik, A.; Saeed, HM Molecular cloning and 3D structure modeling of APEX1, DNA base excision repair enzyme from the Camel. *Camelus dromedarius. Int. J. Mol. Sci.* **2012**, *13*, 8578−8596.
(69) Li, L.; Peng, Y.; Liu, M.; Wang, Z.; Wang, Q.; Ming, S.; Gao, X.; Sun, Y. Apoptosis of human kidney epithelial cells induced by high oxalate and calcium oxalate monohydrate is apurinic/apyrimidinic endonuclease 1 pathway dependent and contributes to kidney stone formation. *Discovery Med.* **2019**, *28*, 75−85.
(70) Lee, SM; Rao, VM; Franklin, WA; Schiffer, MS; Aronson, AJ.; Spargo, BH; Katz, AI IgA nephropathy: morphologic predictors of progressive renal disease. *Hum Pathol* **1982**, *13*, 314−322.
(71) Lee, HS; Lee, MS; Lee, SM; Lee, SY; Lee, ES; Lee, EY; Park, SY; Han, JS; Kim, S.; Lee, JS Histological grading of IgA nephropathy predicting renal outcome: revisiting H. S. Lee's glomerular grading system. *Nephrol Dial Transplant* **2005**, *20*, 342−348.
(72) Zheng, F.; Tang, D.; Li, S.; Luo, Z.; Song, Y.; Huang, Y.; Gan, Q.; Liu, H.; Zhang, X.; Liu, D.; et al. Spatial proteomics landscape and immune signature analysis of renal sample of lupus nephritis based on laser-captured microsection. *Inflamm Res.* **2023**, *72*, 1603−1620.
(73) Wu, T.; Hu, E.; Xu, S.; Chen, M.; Guo, P.; Dai, Z.; Feng, T.; Zhou, L.; Tang, W.; Zhan, L.; et al. clusterProfiler 4.0: A universal enrichment tool for interpreting omics data. *Innovation (Camb)* **2021**, *2*, No. 100141.


https://doi.org/10.1021/acsomega.4c07827
*ACS Omega* 2025, 10, 17208−17220